

The missing links: Evaluating contact tracing with incomplete data in large metropolitan areas during an epidemic

Min-Kyung Chae¹, Woo-Sik Son², and Sang Hoon Lee^{3,*}

¹Department of Physics and Astronomy, Sejong University, Seoul 05006, Republic of Korea

²National Institute for Mathematical Sciences, Daejeon, 34047, Republic of Korea

³Department of Physics and the Research Institute of Natural Science, Gyeongsang National University, Jinju, 52828, Republic of Korea

*lshlj82@gnu.ac.kr

ABSTRACT

Contact tracing (CT) plays a pivotal role in controlling early epidemic spread, particularly when a novel infectious disease emerges. However, the quantitative impact of missing information—such as untraced cases or unnotified contacts—on the effectiveness of CT remains insufficiently understood. Using a stochastic agent-based model with sociodemographics from metropolitan areas in South Korea, we simulate how different forms of information loss affect epidemic spreading dynamics. We construct information-loss scenarios based on two types: infector-omission (IO) and contact-omission (CO), including selective (SCO) and uniform (UCO) scenarios; IO corresponds to the omission of infected individuals (nodes) from the tracing process, leading to the loss of all movement trajectories and downstream transmission links originating from them, whereas CO corresponds to the omission of specific contact events (edges), in which infected individuals are identified but some of their transmission links fail to be detected or notified. The sensitivity of epidemic dynamics to increasing omission rates differs markedly between the two types: IO scenarios exhibit substantially stronger and more abrupt changes in transmission structure and epidemic outcomes, whereas CO scenarios produce more gradual effects. In both scenarios, the magnitude of these effects varies across cities, with a lower-population city (Busan) showing greater tolerance to information loss than the largest city (Seoul), underscoring the importance of regional tailoring in CT strategies. Both IO and CO scenarios also lead to an increase in the transmission network diameter as information loss grows, indicating that a small network diameter reflects effective contact tracing that limits the depth of transmission chains. Collectively, our results offer threshold estimates and practical guidance for designing robust CT systems in the real world.

Introduction

The frequency of major infectious disease outbreaks has increased in the 21st century, with progressively shorter intervals between successive events¹. Among these, the unprecedented COVID-19 pandemic demonstrated that emerging pathogens can severely disrupt not only individual health but also entire economies, education systems, and healthcare infrastructures². When effective vaccines or cures are not available or not widespread, e.g., at the initial period of an epidemic, governments are compelled to rely on a broad arsenal of non-pharmaceutical interventions (NPIs) to mitigate transmission³. First-line responses typically include school closures, teleworking, physical distancing, and contact tracing. When public health systems are overwhelmed, authorities may resort to city lockdowns—measures that are effective in reducing transmission but entail substantial socio-economic costs^{4,5}. Accordingly, even during the early phase of a pandemic, traditional epidemiological responses such as case isolation, movement trajectory reconstruction, and quarantine of contacts remain essential^{6–8}.

Contact tracing (CT) identifies the trajectories of confirmed cases and rapidly finds persons whose paths overlap with those trajectories for testing and quarantine. This approach is especially effective when case numbers are still low⁹. However, CT is far from perfect and remains highly dependent on human resources. Investigators rely on the recollection of individuals to reconstruct trajectories, manually compile contact lists, and request tests and quarantine. These steps inevitably lead to uncertainty and incompleteness—specifically, the inability to trace confirmed cases and the failure to notify contacts. To address these limitations, efforts to improve the accuracy of contact tracing have led to the exploration of various complementary strategies¹⁰. Many countries have experimented with mobile-application-based digital tracing^{11–13}. Despite these efforts, full coverage remains elusive. This limited coverage is often attributed to privacy concerns, varying levels of smartphone adoption, and low user compliance¹⁴.

Quantitative assessments of CT must account for information gaps that arise during real-world implementation. We

developed a high-resolution agent-based model (ABM) to evaluate how such information loss affects CT effectiveness by simulating the spread of emerging infectious diseases across metropolitan areas in South Korea. The model incorporates a multilayer contact network—including households, school classrooms, workplaces, friendships, and local communities. We independently examine two types of information omissions: (1) infector-omission (IO), where the movements and interactions of confirmed individuals are not reconstructed; and (2) contact-omission (CO), where individuals who have been in contact with confirmed cases are not informed in time, which we further distinguish into selective (SCO) and uniform (UCO) scenarios depending on how omissions are distributed across contact networks.

This paper is organized as follows. First, in the “Methods” section, we describe a stochastic ABM based on a synthetic population that reflects the demographic and social contact structure of Seoul (Busan). In the “Results” section, we explain how two types of information omission—IO and CO—are implemented in the model, and we quantitatively analyze their impact on the spread of infection by comparing simulation results between Seoul and Busan. Seoul, the capital of South Korea, is the most populous city in the country. Busan, the second-largest city, has a distinct age distribution compared to Seoul. Finally, in the “Discussion” section, we summarize the strengths and limitations of this study and discuss policy implications for designing effective CT strategies under realistic constraints.

Methods

This section describes our ABM developed to evaluate the effectiveness of CT in response to the emergence of an infectious disease in Seoul (Busan). The model incorporates multilayer social networks¹⁵ to capture heterogeneous interpersonal interactions across different social contexts. Agents carry out typical daily activities—such as going to school, commuting to work, meeting friends, etc.—during which they come into contact with other agents based on realistic schedules. These interactions generate dynamic and diverse contact patterns, allowing the model to simulate the complexity of real-world transmission environments.

Infectious diseases are transmitted through contact between individuals. Therefore, understanding transmission dynamics requires constructing social network models that reflect the underlying interpersonal interaction structure within the population. Given the importance of contact patterns—especially in the context of CT—the ABM is preferable to traditional compartmental models due to its ability to incorporate individual-level heterogeneity^{16,17}. Beyond traditional compartmental models, this individual-level resolution allows our ABM to explicitly reconstruct the directed transmission network. This capability enables us to monitor structural properties such as network diameter, which serves as a proxy for the number of transmission generations, offering deeper insights into spreading dynamics beyond simple prevalence.

We have created a synthetic population reflecting the sociodemographic characteristics of Seoul’s (Busan’s) individuals, which enables more realistic simulations. The model explicitly tracks interactions at the individual level, allowing interpersonal contacts to be distinguished over time.

Agents

We construct the synthetic population to represent the population of Seoul (Busan), matching the population size and incorporating details such as household ID, age, and residence. This is based on the 2020 Korean census data¹⁸ (also used in Chae *et al.*¹⁹), which sampled 2% of the population and was released by the MicroData Integrated Service. We project the 2% census of Seoul (145,817 records) to the entire population of Seoul (9,529,266 agents) using an iterative proportional updating algorithm^{19,20}. We also project the Busan (61,217 records → 3,313,542 agents).

Figure 1(a) illustrates the agent attributes. Each agent is characterized by sociodemographic attributes (e.g., age and residence), social affiliations (e.g., household, school classroom, workplace, friendship, and local community), and epidemiological state (e.g., susceptible, exposed, infectious, and recovered). During the implementation of CT policies, quarantine status is also assigned. The spatial structure of the model reflects the administrative 2 (ADM-2) level regions.

Social Networks

Figure 1(b) shows the multilayer contact network consisting of five social structures:

1. **Households:** Agents belonging to the same household ID are assigned to the same housing unit within a ADM-2 level region. All agents have household IDs.
2. **Workplaces:** We use regional employment rate²¹ to randomly select working-age agents (ages 19–64) from the synthetic population and designate them as workers. The selected agents are assigned the workplace ID and economic districts based on the commuting data. The workplaces are created as many workplace sites, from small offices (mean size = 5 agents) to large offices (mean size = 10 agents), reflecting the distribution of workplace sizes in Seoul (Busan)²². In this model, each worker is associated with a single workplace.

3. **School classrooms:** The method of creating students is almost the same as the method of creating workers. Based on the regional attendance rate^{23–26}, we randomly select school-age agents (ages 3–18) from the synthetic population and designate them as students. The students' classroom IDs and educational districts are assigned using commuting data. Classroom size is determined by the national average number of students per class in Seoul (Busan)^{23–26}. A single teacher is assigned to each classroom, with the number of teachers varying according to class size. All classmates are of the same age. School institutions are not explicitly modeled. The model represents classrooms as isolated units, such that students from different classrooms within the same school do not interact.
4. **Friendships:** A friendship network is generated using a homophilic Barabási-Albert (BA) model^{27,28} that preferentially connects agents of similar age, reflecting the cultural importance of age in Korean social relationships. Agents are organized into age cohorts, each spanning a decade (ages 0–9, 10–19, ..., 80 and older), and the homophilic BA network is generated within each cohort unit. New agents form preferential attachments to existing ones, with a homophily parameter $h = 0.9$ leading to the increased probability of same-age-group links. Each cohort consists of 1,000 agents. Consequently, in this network, agents do not establish links across different cohorts; instead, connections are formed only within the same cohort, with link probabilities determined by same age. This process is applied both within and across administrative regions, resulting in a bidirectional network. Each agent has an average of 20 friends ($\sigma = 13$), ranging from 7 to 228.
5. **Local communities:** Agents living in the same districts are usually connected to simulate casual, short-term encounters in the local community. The connections in the local community network are not static.

Agents follow daily routines according to their demographic profiles (Figure 1(c)). All agents interact with their household members daily. On weekdays, students attend classrooms and workers go to their workplaces. Contacts with friends occur probabilistically, and local community interactions are assigned randomly. Contacts within the friendship network and the local community are modeled stochastically. Each day, every agent independently decides whether to meet friends with a probability of 1/7, and interactions can occur only when both agents choose to do so. As a result, the structure of the friendship network varies from day to day. The local-community layer follows the same mechanism. However, unlike friend gatherings, local-community interactions may involve encounters with unfamiliar individuals as well as acquaintances. Infectious disease spreads through these social interactions across all layers. Further details of the network construction process are provided in the Supplementary Information.

Epidemiological Parameters

We model disease progression using an extended susceptible-exposed-infectious-recovered (SEIR) model described in Figure 2(a). All agents are initially susceptible (S), except for a small number of initially exposed (E) agents. Upon contact with an infector j , a susceptible agent i becomes exposed (E) with a probability of transmission P_{ij} . Among the epidemiological parameters, some values—such as the exposed period, duration of infection, and viral shedding—were adopted from COVID-19 studies^{29–31}, whereas others including the asymptomatic ratio were assumed to be arbitrarily determined. The exposed period (κ) is drawn from a gamma distribution $f(\kappa; \alpha, \theta) = \frac{1}{\Gamma(\alpha)\theta^\alpha} \kappa^{\alpha-1} e^{-\kappa/\theta}$ (shape $\alpha = 1.926$, scale $\theta = 1.775$) for each agent²⁹. Agents in this state are initially non-infectious but become infectious up to two days before entering the infectious state (I)³⁰. Infectiousness is modeled as the product of viral shedding and relative infectiousness. Viral shedding follows a gamma distribution with a mean of 3.067 and a standard deviation of 2.109²⁹. Relative infectiousness (ξ_j) varies across agents, such that some agents exhibit higher or lower overall infectiousness levels. After the exposed state, agents transition to either asymptomatic or symptomatic infectious (I_A or I_S) states with a 20% probability of being asymptomatic ($P_A = 0.2$). All infectious agents are assumed to recover after 8 days ($\eta = 8$)³¹, after which they are no longer infectious. Reinfection is not considered in the study, so that recovered agents gain permanent immunity.

At the end of each simulation day, infection events are determined stochastically. In the study, dt is 1 day. Each S agent i computes the infection risk independently for all contacts with E and I agents j during the day. The probability of transmission P_{ij} per contact is defined as:

$$P_{ij} = 1 - e^{-\lambda_{ij}}, \quad \lambda_{ij} = t_n^{ij} \varphi_j. \quad (1)$$

Here, λ_{ij} represents the force of infection associated with a single contact, and t_n^{ij} is the contact duration based on duration time by location from a Korean social close contact survey³². The distributions of contact duration by location are described in the Supplementary Information. Empirically observed contact durations already reflect relative contact intensities across locations. Accordingly, no additional network-specific scaling factor is introduced in λ_{ij} , and φ_j represents the infectiousness of the infector j . To implement this transmission mechanism, we apply a Monte Carlo sampling procedure based on an

accept–reject scheme. For each contact, a uniform random number is drawn from the interval $[0, 1]$, and infection occurs if this value is less than P_{ij} . This probabilistic procedure enables the model to stochastically determine infection events while preserving the heterogeneity in contact duration and infectiousness. When multiple contacts occur within a day, infection risk is evaluated independently for each contact. The specific numerical values of the epidemiological parameters are summarized in Table 1, and additional details are provided in the Supplementary Information.

Contact Tracing

The CT policy is implemented by tracking the past movement trajectories of confirmed cases to identify individuals who shared space-time overlap with them. Epidemiological investigators check the past movement trajectories of the person who tested positive (confirmed case) and contact people who were in the same location (contacts) to request testing and quarantine.

Figure 2(b) illustrates the decision process of CT, including testing, (self-)quarantine, isolation, and recursive tracing of secondary cases. Symptomatic individuals may initiate self-quarantine before official notification. In this model, 50% of symptomatic agents are assumed to voluntarily seek testing ($P_t = 0.5$). If a symptomatic infected person officially tests positive, the infected person will be isolated and CT will be conducted. If the test result is negative, the self-quarantine will be lifted. Otherwise, individuals (contacts) who are contacted by investigators and are found to have crossed paths with a confirmed case will be tested and placed under precautionary quarantine until their test results are available. Contacts who test negative resume their daily activities. In contrast, those who test positive are isolated, thereby initiating a new round of trajectory checks. The agents are also tested upon release from quarantine, and if they test positive, they are re-isolated. This dynamic and partially voluntary tracing process captures the recursive nature of CT in real-world implementation and allows evaluation of its effectiveness under varying conditions.

In manual CT, epidemiological investigators trace the past movement trajectories of confirmed cases to identify potentially infected individuals. However, this process heavily relies on the memory and cooperation of cases. Since this series of processes is mostly carried out by people, mistakes can occur. As the number of cases increases, the workload for investigators also intensifies, leading to manual CT becoming both resource-intensive and prone to limitations. In practice, these constraints inevitably result in information gaps.

We consider three scenarios with two types of information gaps in manual CT (Figure 3).

- (Scenario 1, IO) An **infector-omission** (IO) scenario occurs when a confirmed case tests positive but their movement trajectory is not traced at all (Figure 3(b)). In the situation, although the case is isolated, all contacts associated with that case remain unidentified and unquarantined.
- (Scenario 2, CO) The second type of information loss corresponds to **contact-omission** (CO), in which agents who have been in contact with confirmed cases are not tested or quarantined. The trajectory of infectors may be available, but investigators fail to notify all agents who overlapped in time and space with the case's trajectory. The results in potentially infected agents moving freely within society, further contributing to disease spread. To capture different patterns of the omission, we consider two distinct contact-omission scenarios:
 - (Scenario 2-1, SCO) A **selective contact-omission** (SCO) scenario occurs when omissions take place only in the friend meeting and local community networks (Figure 3(c)).
 - (Scenario 2-2, UCO) A **uniform contact-omission** (UCO) scenario occurs when omission rates are applied equally across all social networks except the local community network (Figure 3(d)).

In all scenarios, the omission rate for the local community network is fixed at 50%, reflecting the relatively high uncertainty in CT in public spaces. Each scenario is assumed to occur independently, and simultaneous occurrences are not considered.

Results

In our simulations, the three scenarios of information loss are modeled to examine how they affect the effectiveness of CT. Since manual CT is an essential policy in the early stage of an emerging infectious disease outbreak, we assume that the initial number of infectors is small. In the study, the initial infected population is set to 20 agents, each remaining in the exposed (E) state for the first day at the start of the simulation ($E_0 = 20$). The 20 agents are randomly selected from the synthetic population and fixed across all runs. When one of the initially E agents with symptoms visits a hospital and tests positive, the CT policy is initiated. Each simulation is repeated over 100 independent runs to ensure statistical robustness. At the beginning of the simulation, there are no infectious (I) or recovered (R) agents; except for the 20 E agents, all others are susceptible (S). We simulate the outbreak of an emerging infectious disease in virtual Seoul and Busan until it completely disappears. By

Table 1. Summary of parameters and assumptions used in the simulation of CT. The probability density function of the gamma distribution is $f(x; \alpha, \theta) = \frac{1}{\Gamma(\alpha)\theta^\alpha} x^{\alpha-1} e^{-x/\theta}$.

Parameter	Symbol	Value / Distribution	Description
simulation time step	Δt	1 day	time unit of simulation
friend contact probability	—	1/7 per day	daily chance of friends' gathering
local contact probability	—	1/7 per day	daily chance of local random contact
exposed period	κ	$f(x; 1.926, 1.775)$ ²⁹	period from exposure E to infectious I
infectious period	η	8 days ³¹	period from infectious I to recovered R
asymptomatic probability	P_A	0.2	fraction of asymptomatic infectious cases
transmission probability	P_{ij}	$1 - e^{-\lambda_{ij}}$	probability of infection given contact
force of infection	λ_{ij}	$t_n^{ij} \times \varphi_j$	infection risk per contact
contact duration	t_n^{ij}	survey-based	average contact duration per layer, derived from South Korea's social contact survey ³²
infectiousness	φ_j	viral shedding $\times \xi_j$ ³	viral shedding adjusted by individual infectiousness
viral shedding	—	$f(x; 3.067, 2.109)$ ²⁹	baseline viral shedding level of the disease
relative infectiousness	ξ_j	$f(x; 1, 0.5)$ ³	individual infectiousness of infector j
self-testing probability	P_t	0.5	probability that symptomatic agents seek testing voluntarily
quarantine duration	—	1 day	period of quarantine before result
self-quarantine duration	—	1 day	period of voluntary quarantine before result
isolation duration	—	7 days	period of isolation after testing positive
initial exposed agents	E_0	20 (40)	number of initial E population

varying the proportion of missing information in each scenario, we estimate the range of omission rates under which CT can still effectively mitigate the spread of infection, despite being imperfect.

Before presenting the simulation results, we summarize in Table 1 the simulation parameters and behavioral rules implemented in our ABM. These values are applied consistently across all simulations unless otherwise specified. This study assumes the emergence of a novel infectious disease rather than focusing on a specific known pathogen. Accordingly, most epidemiological parameters are assigned arbitrarily. However, values for certain parameters—such as the latent period and duration of infection—are adopted from COVID-19 studies. When a new infectious disease emerges in the future, the model can be easily adapted by updating these epidemiological parameters.

Impact of infector-omission on manual CT effectiveness

The IO scenario captures situations in which some confirmed cases are not traced, leaving their movement trajectories unreconstructed and their contacts unnotified. Although untraced cases are isolated upon confirmation, their contacts continue normal activities, allowing hidden transmission chains to persist. To quantify how IO weakens containment through CT, we simulate outbreaks under varying IO rates, defined as the proportion of confirmed cases whose movement trajectories are not reconstructed by investigators. This setup enables us to evaluate how IO amplifies epidemic spread and to assess the robustness of manual CT under real-world constraints.

We first examine how varying the IO rate affects epidemic magnitude and timing. Figure 4 summarizes the epidemic dynamics in virtual Seoul under varying IO rates. As shown in Fig. 4(a), the mean cumulative number of infections increases sharply once the IO rate exceeds 2%. Figure 4(b) shows the mean epidemic peak time, defined as the time at which the daily number of E agents reaches its maximum. Ideally, aggressive contact tracing leads to rapid containment, causing the epidemic to die out quickly (as shown in the 0% omission rate). As the IO rate increases from 0% to 4%, the system undergoes a transition from a containment phase to an outbreak phase. In the range, the epidemic duration lengthens, and the peak time is delayed not caused by successful mitigation, but rather by persistent infection chains that avoid early stochastic extinction. Once the IO rate exceeds the threshold of 4%, the dynamics shift to a typical epidemic spread where higher transmission potential leads to an earlier and higher peak.

To further examine the structural characteristics of transmission, we analyze the epidemic as a directed transmission network. Each node in the network represents the agent, and a directed edge is drawn from the infector to the infectee, generating the directed transmission network. As the IO rate increases, the mean diameter of the directed transmission network expands significantly before saturating (Figure 4(c)). Here, the diameter of the network refers to the longest chain of infection, that is,

the maximum number of agent-to-agent transmission steps in the network. A larger diameter indicates that the infection chains are penetrating deeper into the population. This ‘deepening’ confirms that the containment policy fails to sever transmission links at an early stage, allowing the outbreak to sustain itself through long, uninterrupted lineages. Figure 4(d) shows the out-degree distribution of the directed transmission network (plotted in the semi-log scale with the log-scale vertical axis). The network denotes the order in which infections occur, with each directed edge indicating a transmission from an infected individual to another individual. This distribution corresponds to the case reproduction number in epidemics, which is defined as the number of secondary infections generated by a single infected individual. In other words, even as the IO rate increases, the nature of the distribution remains largely unchanged. This pattern in the directed transmission network arises because the number of individuals one can meet within a limited time period is structurally constrained.

In Figure 5, we compare epidemic dynamics at an IO rate of 4% with those at 0%. At an IO rate of 0%, infections die out more rapidly, whereas a higher IO rate leads to prolonged transmission. This difference is reflected in the daily incidence trajectories, which show sustained infection at an IO rate of 4% compared to a rapid decline at an IO rate of 0% (Figure 5(a,d)). The corresponding prevalence of the E , I , and R populations further illustrates the persistence of infection under higher IO rates (Figure 5(b,e)). Figure 5(c, f) represents the distribution across social network layers (multilayers) where each infector generates secondary cases. Since the infection spread model has a duration-based transmission probability, most secondary infections occur within households, followed by workplaces, school classrooms, and friend gatherings. Consistent with prior evidence that household transmission constitutes a major component of respiratory disease spread³³. These results demonstrate that our model can realistically produce infection spread patterns under conditions where manual CT is incomplete or partially fails to identify some of the contacts and their transmission pathways.

We then extend the analysis to virtual Busan. Busan has a population of about 1/3 of Seoul, and its age distribution is different³⁴. It has a larger elderly population than Seoul, so the number of workers and students is relatively smaller than in Seoul. In addition, the proportion of workers and students who commute to other areas is about 4.5%pt lower (see, Supplementary Information).

The simulation results in virtual Busan are similar to those in virtual Seoul, despite differences in population structure and demographic characteristics. Figure 6 compares the two cities: the top panel shows results for virtual Seoul, and the bottom panel shows results for virtual Busan. Figure 6(a, c) shows the mean time of the epidemic peak, and Figure 6(b, d) shows the mean epidemic peak height. The thresholds for the IO rate are 4% in virtual Seoul and 10% in virtual Busan. We attribute this to that the three-fold difference in population size is the cause. Despite differences in the precise threshold values due to demographic and population factors, both cities show consistent overall trends in how IO rates affect epidemic dynamics. We examine the effects of IO. We next explain the impact of CO, which represents another major source of information loss in manual CT.

To confirm that these effects are not due to the initial conditions, we double the initial exposed population ($E_0 = 40$) and repeat the same simulations. The results show the same infection spread trend as when $E_0 = 20$ (see, Supplementary Information).

Impact of contact-omission on manual CT effectiveness

The CT also includes requiring testing and quarantine for people whose movements overlap (contacts). However, if the number of confirmed cases becomes too large or staffing is insufficient, investigators may be unable to notify contacts about testing and quarantine in a timely manner. We simulate outbreak dynamics under CO scenarios where contacts are omitted from the notification list. We define the CO rate as the proportion of contacts who fail to receive a testing-and-quarantine notice due to tracing limitations. Two CO scenarios are constructed: (2-1) the SCO scenario, in which only contacts encountered through friend gatherings and local community interactions fail to receive notifications, and (2-2) the UCO scenario, in which contacts across all social networks may fail to be notified. In both scenario, however, the CO rate for the local community network is fixed at 50%, reflecting the relatively high uncertainty in tracing contacts in public spaces.

We simulate the range of SCO rates that contain the spread of infection even if some contacts do not receive tests and quarantines. Figure 7 shows the results of the spread of infection according to the SCO rate in virtual Seoul. The mean cumulative number of infections increases as the SCO rate rises (Figure 7(a)). Figure 7(b) shows that the mean time of the epidemic peak is progressively delayed. In contrast to the IO scenario, which shows a sharp transition, the CO scenario exhibits a continuous delay as the omission rate increases (Figure 7(c)). This suggests that missing contacts does not immediately trigger an explosive outbreak but instead allows infection to spread gradually through the population. As a result, transmission persists without immediate stochastic extinction while avoiding a rapid outbreak. The mean diameter of the directed transmission network does not increase beyond a certain size. In Figure 7(d), the out-degree distribution retains a fat-tailed form. Because not all missed contacts result in secondary infections, increases in the SCO rate lead to less pronounced acceleration of transmission compared with the IO scenario.

In addition, we simulate the UCO scenario that contacts are missed equally in households, school classrooms, workplaces,

and friend gatherings (the omission rate is 50% in the local community). In Figure 8, the top panel shows the results for the SCO scenario (omissions in the friends' gathering and local community networks), whereas the bottom panel illustrates the UCO scenario (omissions across all five network layers). Both CO scenarios exhibit similar overall trends. As the CO rate increases, the mean time of the epidemic peak is delayed, and, the mean epidemic peak height becomes larger. The overall scale of transmission remains smaller than that observed under the IO scenario. These findings suggest that accurately reconstructing the movement trajectories of confirmed cases is more crucial than notifying every contact.

We also repeat the same simulations by doubling the number of initially E agents ($E_0 = 40$). The initial size of the E population has minimal influence on the overall infection dynamics (see, Supplementary Information). Although SCO and UCO have a less pronounced impact than IO, higher omission rates still accelerate transmission and reduce the overall effectiveness of manual CT in containing outbreaks, highlighting the importance of accurate trajectory reconstruction for sustained epidemic control.

Conclusion

The study shows that manual contact tracing (CT) can effectively slow the early spread of emerging infectious diseases, even when some information is missing such as incomplete movement data or unnotified contacts. Using high-resolution agent-based models for Seoul and Busan, we found city-specific thresholds for CT effectiveness: about 4% in Seoul and 10% in Busan. When omission rates exceed these levels, CT quickly becomes ineffective. Among the two types of information loss, missing movement trajectories of confirmed cases had a greater impact on containment than failing to notify all contacts. These results provide practical guidance for prioritizing CT efforts and building tracing systems that can remain effective despite information gaps, helping public health authorities respond more quickly and flexibly to future outbreaks.

Discussion

The study quantitatively analyzed the impact of information loss in manual contact tracing (CT) on quarantine effectiveness during the early phase of an emerging infectious disease outbreak. Using a high-resolution agent-based model (ABM), we generated synthetic populations for Seoul and Busan and simulated two types of information omissions: (1) failure to reconstruct the movement trajectories of confirmed cases (IO), and (2) failure to notify identified contacts for testing and quarantine (CO).

In virtual Seoul, a threshold phenomenon emerged when the IO rate exceeded 4%. Beyond the threshold, epidemic dynamics changed abruptly, showing a rapid increase in the cumulative number of infections, and a finite diameter of the transmission network. In contrast, the two CO scenarios produced more moderate changes, with slower acceleration in transmission even at higher omission rates. These findings indicate that accurately tracing the movement trajectories of confirmed cases plays a more decisive role in containment than complete notification of all contacts. A similar trend was observed in virtual Busan, a city with lower population density and an older demographic structure. However, the IO threshold was higher than that in Seoul (approximately 10% vs. 4%). This difference likely stems from variations in population size, contact density, and commuting intensity. The results suggest that the effectiveness of CT depends on city-specific demographic and social characteristics, implying that tracing strategies should be tailored to reflect regional population and mobility structures³⁵.

The observed delay in peak time at low omission rates serves as an important warning signal. It implies that even modest degradation in trajectory tracking can shift the system from a controlled state toward persistent epidemic growth, turning a manageable containment phase into an uncontrolled outbreak. In comparison, failures in CO produce a more gradual shift in epidemic timing, reinforcing the conclusion that accurate trajectory reconstruction is the primary driver of containment success. This disparity arises because missing an infector (IO) leaves an entire transmission chain invisible, effectively retaining the connectivity of the transmission network, whereas missing a contact (CO) only preserves a single link. Consequently, trajectory reconstruction acts as a root-level intervention, essential for keeping the effective reproduction number below unity.

A distinct contribution of the study is the topological analysis of the transmission network via its diameter. We observed that incomplete trajectory tracking leads to a drastic increase in the diameter, signaling prolonged transmission chains. While epidemic size indicates the immediate disease burden, a large diameter implies that the virus undergoes more replication cycles through successive transmission events. This structural deepening could theoretically elevate the risk of emerging variants of concern by providing more opportunities for mutation accumulation within extended transmission chains.

Nonetheless, the study has several limitations. First, our model simulations were not based on actual CT logs or epidemiological investigation data, but were instead constructed from census microdata, social contact survey data, and other statistical sources to create synthetic yet realistic contact networks³⁶. As such, we were unable to quantitatively validate the realism or accuracy of the CT processes reproduced by the model. Additionally, in reality, CT requires an initial preparation phase, during which some delay inevitably occurs before tracing the first confirmed cases. The delay was not reflected in our simulations. Third, dynamic changes in individual behavior or government policy responses over time were not incorporated. These assumptions do not fully capture the complexity of how such omissions occur in real-world CT operations. To address

these limitations, future work should incorporate actual CT logs or investigation records for model validation and explore policy scenarios that include adaptive behavioral and governmental responses.

Despite these limitations, our study presents quantitative estimates of the impact and threshold levels of CT information loss through city-scale, high-resolution simulations. Our findings provide a practical foundation for designing efficient CT strategies under constrained resources. Simulation-based analyses such as this can support public health decision-making by helping to define acceptable levels of information loss and prioritize response actions. In future research, the infection spread model may be extended to incorporate vaccination coverage, the transmissibility of emerging variants, and digital tracing technologies, enabling more refined and policy-relevant epidemic assessments.

Data availability

The simulation codes supporting the findings of this study are available at https://github.com/MkChae/ABM_CT. All input data required to reproduce the simulations, including synthetic population data, are available at https://drive.google.com/drive/folders/1--0Iw4U4nhQS6YCv9TYgYYEJgUTt1Gz6?usp=share_link.

References

1. Daszak, P. & Jones, K. Global trends in emerging infectious diseases. *Nature* **451**, 990–993 (2008).
2. Naidoo, R. & Fisher, B. Reset sustainable development goals for a pandemic world. *Nature* **583**, 198–201 (2020).
3. Ferguson, N. M. *et al.* Strategies for containing an emerging influenza pandemic in southeast asia. *Nature* **437**, 209–214 (2005).
4. Hellewell, J. *et al.* Feasibility of controlling COVID-19 outbreaks by isolation of cases and contacts. *The Lancet Glob. Heal.* **8**, e488–e496 (2020).
5. Gilbert, M., Dewatripont, M., Muraille, E., Platteau, J.-P. & Goldman, M. Preparing for a responsible lockdown exit strategy. *Nat. medicine* **26**, 643–644 (2020).
6. Kucharski, A. J. *et al.* Effectiveness of isolation, testing, contact tracing, and physical distancing on reducing transmission of sars-cov-2 in different settings: a mathematical modelling study. *The Lancet infectious diseases* **20**, 1151–1160 (2020).
7. Fraser, C., Riley, S., Anderson, R. M. & Ferguson, N. M. Factors that make an infectious disease outbreak controllable. *Proc. Natl. Acad. Sci.* **101**, 6146–6151 (2004).
8. Cai, Y. *et al.* Assessing the effectiveness of test-trace-isolate interventions using a multi-layered temporal network. *Infect. Dis. Model.* **10**, 775–786 (2025).
9. Cetron, M., Maloney, S., Koppaka, R. & Simone, P. Isolation and quarantine: containment strategies for sars 2003. *Learn. from SARS: preparing for next disease outbreak* 71–83 (2004).
10. Kojaku, S., Hébert-Dufresne, L., Mones, E., Lehmann, S. & Ahn, Y.-Y. The effectiveness of backward contact tracing in networks. *Nat. physics* **17**, 652–658 (2021).
11. Ferretti, L. *et al.* Quantifying SARS-CoV-2 transmission suggests epidemic control with digital contact tracing. *science* **368**, eabb6936 (2020).
12. Almagor, J. & Picascia, S. Exploring the effectiveness of a COVID-19 contact tracing app using an agent-based model. *Sci. reports* **10**, 22235 (2020).
13. Lopera González, L. I., Köber, G., Kirchner, G., Benzler, J. & Amft, O. Impact of digital contact tracing on pandemic control analysed with behaviour-driven agent-based modelling. *medRxiv* 2025–01 (2025).
14. Altmann, S. *et al.* Acceptability of app-based contact tracing for COVID-19: Cross-country survey study. *JMIR mHealth uHealth* **8**, e19857 (2020).
15. Kivelä, M. *et al.* Multilayer networks. *J. Complex Networks* **2**, 203–271, DOI: [10.1093/comnet/cnu016](https://doi.org/10.1093/comnet/cnu016) (2014). <https://academic.oup.com/comnet/article-pdf/2/3/203/9130906/cnu016.pdf>.
16. De Marchi, S. & Page, S. E. Agent-based models. *Annu. Rev. Polit. Sci.* **17**, 1–20 (2014).
17. Rahmandad, H. & Sterman, J. Heterogeneity and network structure in the dynamics of contagion: Comparing agent-based and differential equation models. In *Proceedings of the 22nd International Conference of the System Dynamics Society* (System Dynamics Society Oxford, UK, 2004).
18. MDIS. 2% census in South Korea (in Korean). *statistics* <https://mdis.kostat.go.kr/eng/index.do> (2020).

19. Chae, M.-K., Hwang, D.-U., Nah, K. & Son, W.-S. Evaluation of COVID-19 intervention policies in south korea using the stochastic individual-based model. *Sci. Reports* **13**, 18945 (2023).
20. Ye, X., Konduri, K., Pendyala, R. M., Sana, B. & Waddell, P. A methodology to match distributions of both household and person attributes in the generation of synthetic populations. In *88th Annual Meeting of the transportation research Board, Washington, DC*, vol. 36 (2009).
21. KOSIS. Working-age population by age (in Korean). *statistics* https://kosis.kr/statHtml/statHtml.do?orgId=101&tblId=DT_1DA7015S&conn_path=I2 (2023).
22. KOSIS. Number of businesses by employee size (in Korean). *statistics* https://kosis.kr/statHtml/statHtml.do?orgId=101&tblId=DT_1K52D03&conn_path=I2 (2022).
23. KOSIS. Kindergarten overview (in Korean). *statistics* https://kosis.kr/statHtml/statHtml.do?orgId=334&tblId=DT_1963003_001&conn_path=I2 (2023).
24. KOSIS. Elementary school overview (in Korean). *statistics* https://kosis.kr/statHtml/statHtml.do?orgId=334&tblId=DT_1963003_002&conn_path=I2 (2023).
25. KOSIS. Junior school overview (in Korean). *statistics* https://kosis.kr/statHtml/statHtml.do?orgId=334&tblId=DT_1963003_003&conn_path=I2 (2023).
26. High school overview (in Korean). *statistics* https://kosis.kr/statHtml/statHtml.do?orgId=334&tblId=DT_1963003_004&conn_path=I2 (2023).
27. Lee, E. *et al.* Homophily and minority-group size explain perception biases in social networks. *Nat. Hum. Behav.* **3**, 1078–1087 (2019).
28. Barabási, A.-L. & Albert, R. Emergence of scaling in random networks. *Science* **286**, 509–512 (1999).
29. He, X. *et al.* Temporal dynamics in viral shedding and transmissibility of COVID-19. *Nat. Medicine* **26**, 672–675 (2020).
30. Sun, K. *et al.* Transmission heterogeneities, kinetics, and controllability of sars-cov-2. *Science* **371**, eabe2424 (2021).
31. Wölfel, R. *et al.* Virological assessment of hospitalized patients with COVID-2019. *Nature* **581**, 465–469 (2020).
32. Son, W.-S. *et al.* Social contact patterns in south korea: an analysis of a survey conducted in 2023-2024. *BMC Infect. Dis.* **25**, 295 (2025).
33. Madewell, Z. J., Yang, Y., Longini, I. M., Halloran, M. E. & Dean, N. E. Household transmission of sars-cov-2: a systematic review and meta-analysis. *JAMA network open* **3**, e2031756–e2031756 (2020).
34. Kim, D. Exploratory study on the spatial relationship between emerging infectious diseases and urban characteristics: Cases from korea. *Sustain. Cities Soc.* **66**, 102672 (2021).
35. Zhang, K. *et al.* Evaluating the impact of test-trace-isolate for COVID-19 management and alternative strategies. *PLOS Comput. Biol.* **19**, e1011423 (2023).
36. Kerr, C. C. *et al.* Covasim: an agent-based model of COVID-19 dynamics and interventions. *PLOS Comput. Biol.* **17**, e1009149 (2021).
37. FLATICON. <https://www.flaticon.com>. Accessed: 2025-07-37.

Acknowledgements

This work was supported by the National Institute for Mathematical Sciences (NIMS) under Grant No. NIMS-B26730000 (W.-S.S.) and by the National Research Foundation of Korea (NRF) under Grant No. RS-2021-NR061247 (S.H.L.).

Author contributions statement

M.-K.C. and W.-S.S. designed the study. M.-K.C. developed the model and conducted the simulations. M.-K.C. and S.H.L. analyzed the results. All authors conducted the literature review, wrote the manuscript, and reviewed the manuscript.

Competing interests

The authors declare no competing interests.

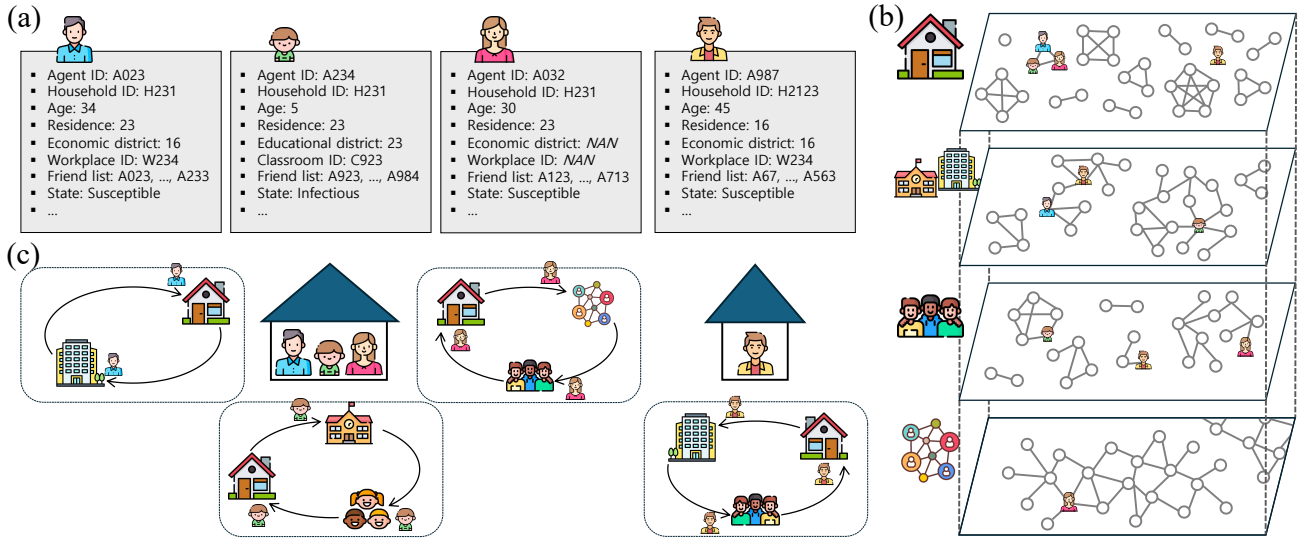


Figure 1. (a) Schematic representation of each agent's sociodemographic attributes, including household ID, age, residence, workplace and school classroom affiliation, and epidemiological status. (b, c) Example of a contact network generated by daily behavior patterns over a single day. (b) Multilayer contact network comprising household, workplace/classroom, friendship, and local community interactions. Each layer captures the social connection among agents. (c) Example of a daily routine for each agent. Agents follow different schedules depending on their demographic characteristics, such as attending school, going to work, or interacting with friends and community members. The agent icons were sourced from FLATICON³⁷.

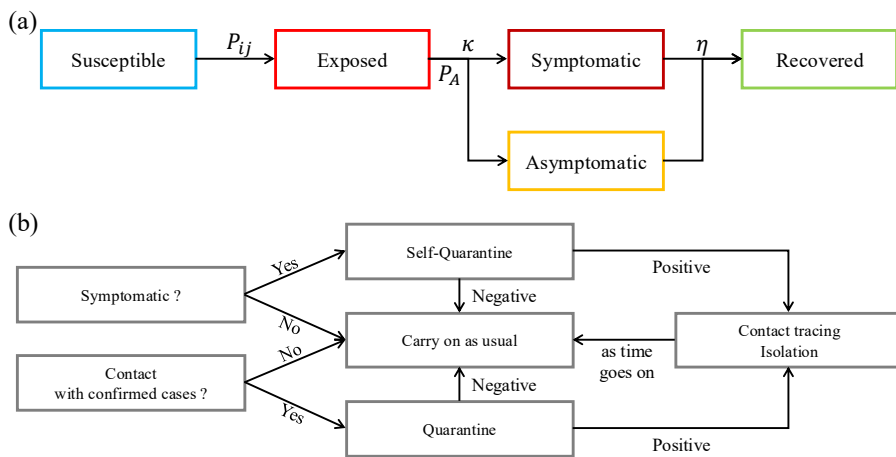


Figure 2. (a) Progression of an infectious disease through five states: susceptible (S), exposed (E), symptomatic infectious (I_S), asymptomatic infectious (I_A), and recovered (R). A susceptible agent becomes exposed with transmission probability P_{ij} upon contact with an infector ($S \rightarrow E$). After κ days in the exposed state, agents transition to either I_S or I_A (P_A), and recover after η days. (b) Schematic representation of the CT protocol, illustrating the pathways of symptomatic agents and exposed contacts through testing, (self-)quarantine, isolation, and secondary contact identification.

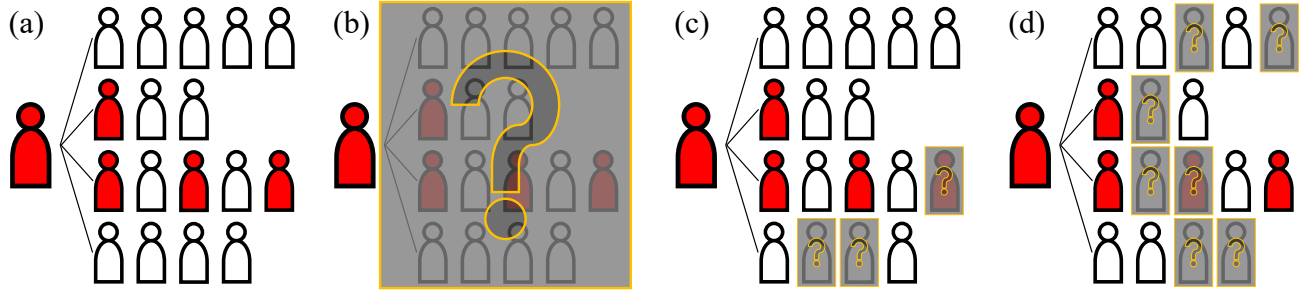


Figure 3. Illustration of information-gap scenarios in manual CT. The red agents represent infected individuals, the white agents represent uninfected agents, and the agents shaded in gray with the question mark (regardless of colors inside) indicate omitted agents. (a) Ideal CT with full trajectory tracing and complete identification of contacts. (b) Infector-omission (IO): the confirmed case's trajectory is not traced, leaving all contacts unidentified. (c) Selective contact-omission (SCO): only contacts in friends' gathering and local community networks are partially missed. (d) Uniform contact-omission (UCO): omissions occur across all networks.

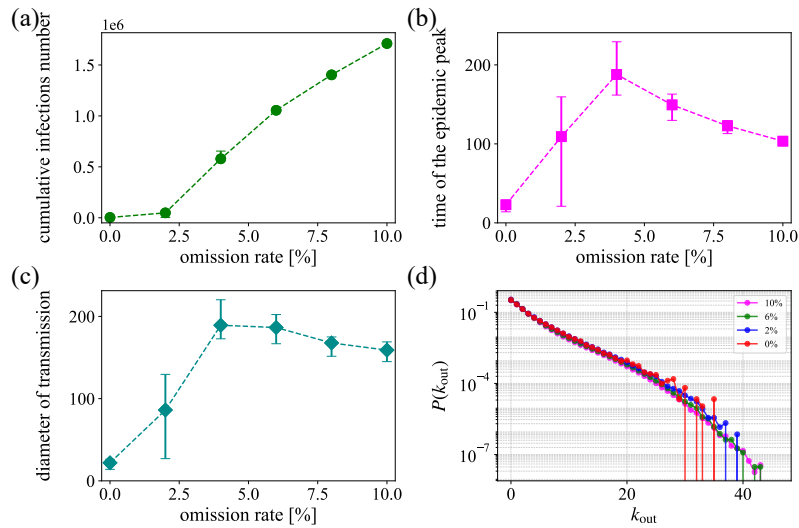


Figure 4. Simulation results of the spread of infection by IO rate in a virtual Seoul ($E_0 = 20$, with a 50% confidence interval (CI)): (a) the mean cumulative number of infections, (b) the mean time of the epidemic peak, (c) the mean diameter of the directed transmission network, and (d) the out-degree distribution of the directed transmission network (with the log-scale vertical axis). The colors represent IO rate of 0% (red), 2% (blue), 4% (green), and 10% (magenta), respectively.

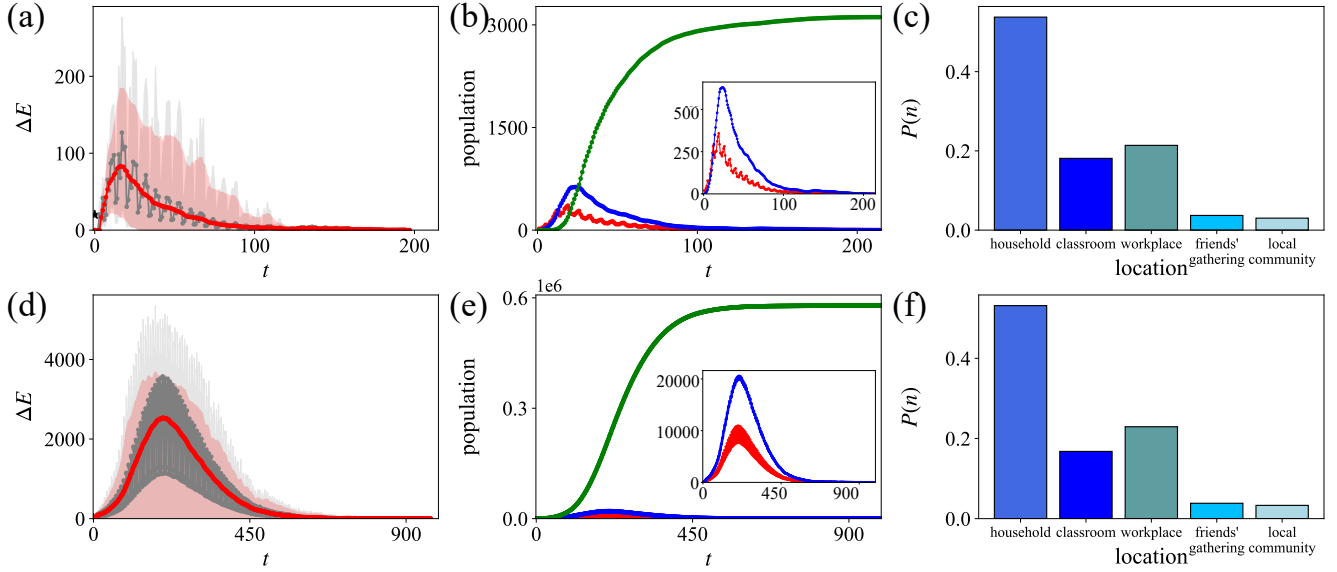


Figure 5. Simulation results of the spread of infection in Seoul when the initial number of confirmed cases is 20: the IO rate (a–c) 0% and (d–f) 4%. (a, d) The daily number of E agents with a 90% CI shown as shaded areas. The gray line is the daily incidence of infection. The red line results from a 7-day moving average on the daily incidence of infection. The black star symbol denotes initial exposed population ($E_0 = 20$). (b, e) Prevalence of E (red), I (blue), and R (green) population. (c, f) Distribution of probabilities for the types of locations in which each infector causes secondary transmissions.

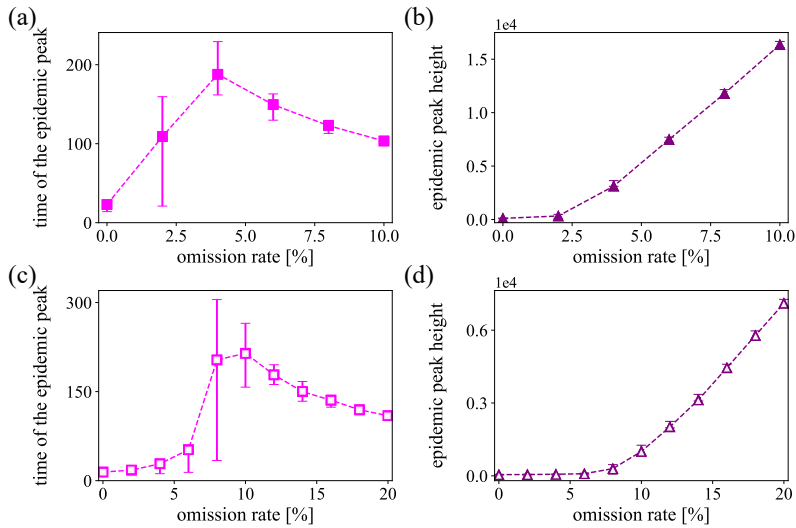


Figure 6. Simulation results of infection spread in virtual (a, b) Seoul and (c, d) Busan by IO rate ($E_0 = 20$, with a 50% CI): (a, c) the mean time of the epidemic peak, and (b, d) the mean epidemic peak height.

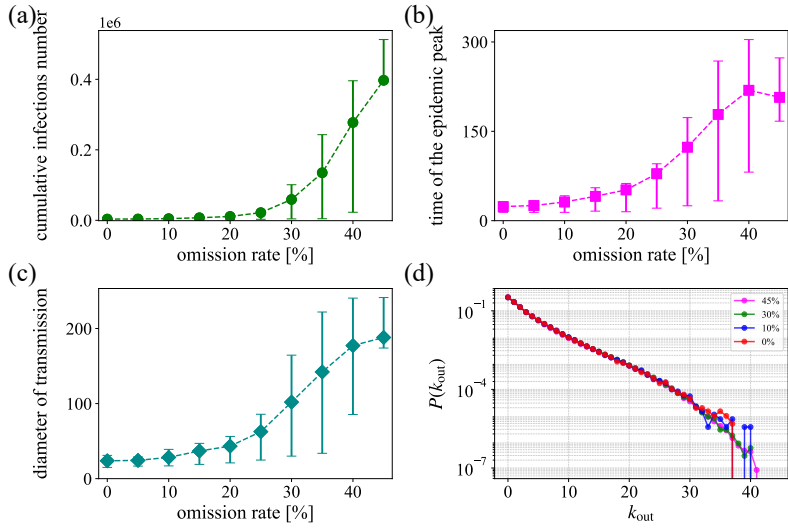


Figure 7. Simulation results of the spread of infection by SCO rate in a virtual Seoul ($E_0 = 20$, with a 50% CI): (a) mean cumulative infections number, (b) the mean time of the epidemic peak, (c) the mean diameter of the directed transmission network, and (d) the out-degree distribution of the directed transmission network (with the log-scale vertical axis). The colors represent SCO rate of 0% (red), 10% (blue), 30% (green), and 45% (magenta), respectively.

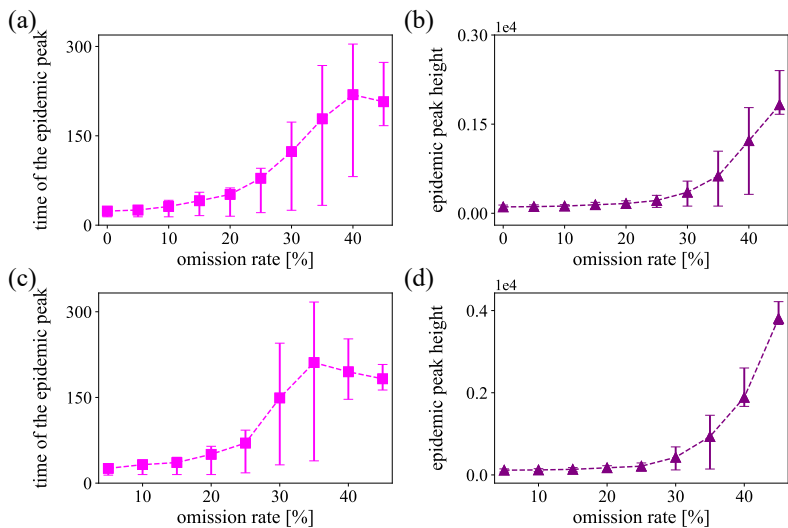


Figure 8. Simulation results under varying CO rates in virtual Seoul for two CO scenarios ($E_0 = 20$, with a 50% CI). Top panels show the results of the SCO scenario, and bottom panels show the results of the UCO scenario. Left panels present the mean time of the epidemic peak, whereas right panels present the mean epidemic peak height.